

ARTICLE

Correlation of the ratio of metallic to oxide species with activity of PdPt catalysts for methane oxidation

Tang Son Nguyen^{a,b*}, Paul McKeever^a, Miryam Arredondo-Arechavala^c, Yi-Chi Wang^d, Thomas J. A. Slater^e, Sarah J. Haigh^d, Andrew M. Beale^{f*}, Jillian M. Thompson^{a*}

Received 00th January 20xx,
Accepted 00th January 20xx

DOI: 10.1039/x0xx00000x

Bimetallic catalysts consisting of Pd and Pt on TiO₂-zeolite (mordenite, beta, ZSM-5) supports were prepared and tested for the combustion of methane. The activity of the catalysts was found to be dependent on the zeolite topology and SiO₂:Al₂O₃ ratio and was linearly dependent on the proportion of Pd and Pt present in a bimetallic phase observed in XRD diffractograms of the catalysts. This linear dependence was valid for a range of zeolites used. STEM-EDS and electron tomography showed the Pd and Pt to be largely co-located and XAS and XPS indicated that the metals are mostly present in the form of oxide nanoparticles with a minor contribution from the metals at high SiO₂:Al₂O₃ ratios. Catalyst characterization showed there to be little difference overall in the metal loading and physical characteristics of the samples and NH₃-TPD suggested that the activation of methane over acid sites is not important. Adding water to the feed, slightly reduced the conversion but did not affect the deactivation profile of the catalysts tested.

1. Introduction

Natural gas has gained popularity in transport, power generation and heating applications due to its abundance, versatility and high calorific value. Methane is available from a number of sources including oil reserves, as shale gas and is generated from renewable sources by digestion of biomass. However it has a greenhouse gas potential 20 to 100 times higher than that of CO₂¹. Thus, incomplete combustion is not only a waste of resource but also causes severe environmental issues. Although methane should burn to give only CO₂ and H₂O, due to its highly symmetrical structure, and consequently high stability, activation of the combustion reaction requires either high temperature or the presence of a catalyst. In thermal combustion, the high temperature results in the formation of various pollutants including NO_x, CO as well as an unburned portion.² Catalytic combustion of methane operating at lower temperatures not only requires less energy input but also reduces the emission of pollutants making it an efficient and

less environmentally damaging strategy for methane utilization.^{3,4} Low temperature catalytic methane combustion has received increased interest specifically in the area of after treatment for emissions from natural gas-powered vehicles.^{5,6} Increasingly stringent European legislation requiring separate monitoring of methane and non-methane hydrocarbons from vehicles means that many natural gas and dual fuel powered vehicles no longer meet these requirements. Development of a catalyst to allow abatement of these emissions is vital for the utilisation of methane in transportation in the future.⁷

It is widely agreed that Pd-based materials are the most active catalysts for methane combustion³, with a number of studies using Pd-based catalysts showing considerable activity below 300 °C⁸⁻¹⁰. The mechanism by which methane combustion occurs over Pd catalysts has been proposed to proceed *via* the dissociative adsorption of methane on metallic Pd to form methyl surface species, which are subsequently oxidised into the final products by the presence of PdO.^{11,12} Thus, an intricate balance between the metallic and oxide forms of Pd on the surface appears to be a requisite for high activity and stability. Zeolites are often employed as a support for methane combustion catalysts and besides their role as a dispersion media, the surface acidity of zeolites has also been shown to influence the catalytic activity.¹³⁻¹⁶ It was proposed that the C-H bond in short-chain alkanes could be activated *via* protolysis at low temperatures over the Brønsted acid sites of zeolite.¹⁷ However, Dai *et al.* comprehensively studied the role of different acid sites in the catalytic combustion of methane over PdO/H-ZSM-5 catalysts and it was confirmed that the role of Brønsted acid sites on the direct activation of methane was negligible.¹⁸ In the same study, the dispersion of PdO was shown to be dependent on acid sites of supports and the influence of Lewis acid sites in particular was considered more decisive (i.e.

^a School of Chemistry and Chemical Engineering, Queen's University Belfast, Belfast BT9 5AG, Northern Ireland, UK

^b Faculty of Biotechnology, Chemistry and Environmental Engineering, PHENIKAA University, Hanoi 10000, Vietnam

^c Centre for Nanostructured Media, School of Mathematics and Physics, Queen's University Belfast, University Road, Belfast BT7 1NN, UK

^d School of Materials, University of Manchester, Oxford Road, Manchester M13 9PL, UK

^e Electron Physical Sciences Imaging Centre, Diamond Light Source Ltd., Oxfordshire OX11 0DE, UK

^f Department of Chemistry, University College London, 20 Gordon Street, London WC1H 0AJ, U.K., & Research Complex at Harwell, Rutherford Appleton Laboratory, Didcot OX11 0FA, UK

Electronic Supplementary Information (ESI) available: [BET plot; NH₃-TPD profiles; SEM images; STEM-HAADF reconstructions; EXAFS fitting and parameters; XPS peak positions; characterisation of fresh and aged catalysts; activity and stability tests with water in the feed stream]. See DOI: 10.1039/x0xx00000x

through dispersion and stabilization of PdO_x)¹⁸. Okumura *et al.* further confirmed the role of the acid sites in H-ZSM-5 in controlling the dispersion and thus the activity of palladium in methane combustion¹⁶. It was proposed that PdO species were anchored on the acid sites of the zeolite support through acid-base interactions, consequently leading to higher stability and smaller Pd particles being achieved with H-ZSM-5 supports of lower SiO₂:Al₂O₃ ratios. One of the key findings of this study was the dependence of catalytic activity on the SiO₂:Al₂O₃ ratio of the H-ZSM-5 support, which spans from 24 to 1000. The activity was shown to increase with the SiO₂:Al₂O₃ ratio, reaching a maximum at a value of 200 before decreasing. Interestingly, these results suggest that initially the activity of the PdO/H-ZSM-5 catalyst is inversely proportional to PdO dispersion up to a SiO₂:Al₂O₃ ratio of 200. The authors finally concluded that the activity of Pd for methane combustion followed the order: PdO dispersed < PdO agglomerated << mixture of Pd metal and PdO¹⁶. Lou *et al.* employed different experimental techniques in combination with DFT calculations to study the active site in low-temperature methane combustion over a Pd/H-ZSM-5 catalyst¹⁰. It was shown that [AlO₂]Pd(OH)-ZSM-5 sites, formed by the interaction between PdO_x and the surface Brønsted acid sites of H-ZSM-5 are likely the active species in the catalyst. Furthermore, the catalytic activity increases with an increase in the Pdⁿ⁺ /Pd²⁺ ratio (0 < n < 2), suggesting that Pd species with lower oxidation states will benefit the activity for methane combustion¹⁰.

Osman *et al.* reported the utilization of H-ZSM-5 and TiO₂ as a dual component support for a bimetallic Pd-Pt catalyst which resulted in a methane combustion catalyst with activity below 250 °C.¹⁹ It was noted that the presence of Pt enhanced the activity and stability of the catalyst. The use of TiO₂ on the support, was reported to assist in the transport of oxygen for the oxidation of Pd and also in facilitating the reduction of PdO to Pd metal and thus maintaining sufficient sites for dissociative methane adsorption. The importance of sonication in the catalyst synthesis was attributed to ensuring thorough mixing of catalyst components, required for high activity, however, the distribution of the metals on the TiO₂ and zeolite was not clear. The acidity of H-ZSM-5 was also shown to influence the activity of the bimetallic catalysts, however, this was not systematically studied. The observation of an optimum TiO₂ loading and zeolite acidity highlights the fine balance of catalyst components required for optimised activity; an improved understanding of the role of the support acidity and the distribution of catalyst components provides the motivation for the current study.

In this current work, catalysts comprising of Pd, Pt and TiO₂ with zeolite supports of different topologies and H-ZSM-5 supports of different SiO₂:Al₂O₃ ratios were synthesized using the composition optimised previously.¹⁹ A comprehensive range of characterization techniques were employed to further understand the interaction and distribution of catalyst components as well as the influence of the acidity of the support on the catalytic activity in the methane combustion reaction.

2. Experimental

2.1 Materials

The materials used to prepare and characterise the catalysts as well as test their activity were analytical grade and were used as received. Palladium (II) nitrate dihydrate (Pd(NO₃)₂·2H₂O, ~40 % Pd basis) and titanium (IV) oxide anatase nanopowder (TiO₂, 99.7 % anatase) were obtained from Sigma-Aldrich. Tetraammine platinum (II) hydroxide in solution (Pt(NH₃)₄(OH)₂, assay 9.09 %) was obtained from Alfa Aesar as were the samples of the MFI framework zeolite ZSM-5 (SiO₂:Al₂O₃ 23:1, 30:1, 50:1 and 80:1 molar ratio), mordenite (SiO₂:Al₂O₃ of 20:1), and beta (SiO₂:Al₂O₃ of 38:1). All gases (Ar, 20 % O₂/Ar, CH₄, NH₃/Ar, N₂, Ne) were obtained from BOC and had 100% purity.

2.2 Preparation of Palladium/Platinum catalysts.

The catalysts were prepared using wet impregnation. Typically, zeolite (1.51 g) was placed in a beaker with an appropriate amount of precursor to result in a catalyst with 5 wt.% Pd, 2 wt.% Pt and 17.5 wt.% TiO₂. Deionised water (~5 mL) was added to the beaker which was placed in an ultrasonic bath (Crest 200 HT) and sonicated at 80 °C using a frequency of 45 kHz for 3 hours. All mixtures were then evaporated to dryness in an oven at 110 °C overnight and calcined in air at 550 °C for 4 h with a heating ramp of 1 °C min⁻¹. Herein the catalysts are referred to as Pd,Pt,TiO₂/zeolite according to the zeolite support, which includes H-ZSM-5, H-MOR and H-BEA with their SiO₂:Al₂O₃ ratio given in brackets e.g. the catalyst sample with Pd and Pt on the H-ZSM-5 zeolite support with a SiO₂:Al₂O₃ ratio of 23:1, is referred to as Pd,Pt,TiO₂/H-ZSM-5(23). The weight percentages are assumed to be 5 wt.% Pd, 2 wt.% Pt and 17.5 wt.% TiO₂ unless otherwise stated.

After drying the catalyst at 110 °C but not calcining in air, a sample was pre-reduced by heating in H₂ to 100 °C. This temperature is lower than that required for the reduction of TiO₂ but higher than that required for the reduction of PdO. This catalyst was then heated in Ar to 550 °C before cooling to room temperature and then calcined at 550 °C as described above.

2.3 Catalyst Characterization

Surface areas and pore volumes of the supports and catalysts were obtained using Brunauer-Emmett-Teller (BET) analysis which included criteria proposed by Rouquerol *et al.*²⁰ (ESI 1). The data, measured by the N₂ adsorption and desorption isotherm at -196 °C, at relative pressures below 0.1 were obtained on a Micromeritics TriStar II 3020 system.

ICP analysis was carried out using an Agilent Technologies 5100 ICP-OES system, with the samples being prepared by sodium peroxide fusion and dissolution in acid before analysis.

Powder X-ray diffractograms (XRD) were obtained on a PANalytical X'Pert Pro X-ray diffractometer, equipped with a Cu K_α X-ray source of wavelength 1.5406 Å. The X-ray tube was set at 40 kV and 40 mA and data collected between 5 and 80 ° 2θ. Peaks were identified by comparison with diffraction patterns in the software library as well as with zeolite standard samples. The PdO crystallite size was calculated from the reflection (101)

at $34.6^\circ 2\theta$ using the Scherrer Equation, in which the peak width at half maximum intensity was calculated by the peak fitting function in the programme Highscore Plus.

Ammonia temperature-programmed desorption (NH_3 -TPD) and temperature-programmed reduction (TPR) data were obtained on a Micromeritics Autochem II apparatus with the H_2 uptake monitored by a thermal conductivity detector (TCD). Typically for NH_3 -TPD, a sample of catalyst (0.1 g) was degassed at 550°C under a 50 mL min^{-1} flow of Ar for 1 h (with a heating rate of 5°C min^{-1}) then; the sample was cooled to 100°C and saturated with a 50 mL min^{-1} flow of 2% NH_3/Ar for 0.5 h. The sample was then purged with argon, at 100 mL min^{-1} for 45 min, to remove weakly and physically adsorbed NH_3 on the surface of the catalyst. Finally, the sample was heated at a rate of 5°C min^{-1} under a 50 mL min^{-1} flow of Ar from 100°C to 600°C and the amount of NH_3 in the effluent was measured via the TCD. For the TPR analysis, Ar was flowed over the sample until the temperature was decreased to 50°C . 5% H_2/Ar was then passed over the catalyst at 30 mL min^{-1} until a stable baseline was obtained when the sample was heated at $10^\circ\text{C min}^{-1}$ up to 600°C .

Transmission electron microscope (TEM) characterisation was performed using a Thermo Fisher Talos F200X G2 fitted with the Super-X energy dispersive X-ray spectrometer (EDS) detector configuration having a total collection angle of ~ 0.9 sr and operated at 200 kV using high angle annular dark field (HAADF) scanning TEM (STEM) and EDS. The Si-K, Al-K, Ti-K, Pt-L and Pd-L peaks were used to generate the EDS elemental maps. The samples did not undergo any pre-treatment before analysis.

High resolution STEM-HAADF images shown in Figure 6 were acquired using a probe-corrected Thermo Fisher Titan G2 80-200 S/TEM operated at 200 kV, and equipped with an X-FEG high brightness source and STEM probe aberration corrector.

STEM-HAADF tomography acquisition was performed with a Fischione 2020 tomography holder in the same Thermo Fisher Talos STEM instrument. The accelerating voltage was 200 kV, probe current ~ 80 pA, EDS pixel dwell time $40\ \mu\text{s}$ with total scan frames for spectrum images of 100 frames (frame size 512×512). For low magnification tomography, the tilting range was from $+78^\circ$ to -72° with 2° increments and a pixel size of 0.47 nm . Pixel sizes were binned to 0.94 nm for reconstruction. For high magnification tomography, the tilting range was from -76° to 74° with 2° increments and a pixel size of 0.11 nm . Dwell time is $10\ \mu\text{s}$. In the Tomviz reconstruction software²¹, images and tilt axes were aligned automatically and image intensities were normalised before using the Total Variation Minimization (TVM) reconstruction method²² applied with 10 iterations.

X-ray absorption fine structure (XAFS) studies were performed at the B18 beamline at the Diamond Light Source in Harwell, United Kingdom. The X-ray energy was 3 GeV and the ring current 300 mA. Pd K and Pt L_{III}-edges were recorded in transmission mode using ion chamber detectors with a fast scanning Si (111) double crystal monochromator. The acquisition of each spectra took ~ 60 s, with the respective metal foils placed between I_t and I_{ref} . The dimension of the X-ray beam used was $1 \times 1\text{ mm}^2$. X-ray absorption spectroscopy

(XAS) data analysis was performed using the Demeter software package.²³

X-ray photoelectron spectroscopy (XPS) was performed on a Kratos AXIS Supra spectrophotometer, equipped with a monochromatic Al K α source (1486.7 eV) and a charge neutraliser. Spectra were processed with CasaXPS software version 2.3.16 and Origin software version 8.6 and quantified after Shirley background correction and application of relevant response factors to quantification regions.

2.4 Catalyst activity

The activity of the catalysts for methane oxidation was tested in a stainless steel fixed-bed reactor ($\frac{1}{4}$ " outer diameter) at atmospheric pressure. The catalyst (0.108 g), was sieved to between 250 and 425 μm and was placed centrally in the reactor between two plugs of quartz wool with an Omega thermocouple placed in the centre of the bed to monitor the reaction temperature. The flow of Ar, O_2/Ar and Ne to the reactor was controlled using Aalborg mass flow controllers, whilst that of CH_4 was controlled by a Bronkhorst mass flow controller. The catalyst was heated at a rate of 5°C min^{-1} to 500°C for 2 h under a flow of 5% O_2/Ar (40 mL min^{-1}), before the reaction mixture, containing 0.5% CH_4 , 10% O_2 , 5% Ne (used as internal standard) and 84.5% Ar, was added to the reactor. The total flow was maintained at 180 mL min^{-1} , giving a gas hourly space velocity (GHSV) of $100,000\text{ mL g}^{-1}\text{ h}^{-1}$.

The stability of all catalysts was tested using the same conditions as given above but the temperature was maintained at 300°C for 35 hours, except for the Pd,Pt,TiO₂/H-ZSM-5 (80) material, which was tested for 50 hours.

To evaluate the catalysts in the presence of water, the reaction stream was passed through a water saturator at a temperature to give a composition of 0.48% CH_4 , 9.5% O_2 , 4.8% Ne, 80.5% Ar and 4.8% H_2O (9 mL min^{-1}), and a GHSV of $105,000\text{ mL h}^{-1}\text{ g}^{-1}$.

The products were analysed by on-line gas chromatography (GC) using an Agilent 7820A GC equipped with a methanizer, a TCD and a Flame Ionisation Detector (FID) using a PoraPlotQ column. Under the conditions used, an exotherm was observed due to the exothermic nature of the methane combustion reaction, in which a temperature gradient of up to 10°C was found between the centres of the furnace and the catalyst bed at high conversions.

Rates of reaction were measured at steady temperatures from 500°C to 200°C . The percentage methane conversion was calculated based on the flow rates of reacted and unreacted methane. All activity data were measured under dry conditions unless otherwise stated.

$$\% \text{ conversion} = \frac{\left(\frac{F_{\text{CH}_4,\text{in}}(\text{molmin}^{-1})}{F_{\text{Ne}}(\text{molmin}^{-1})} \right) - \left(\frac{F_{\text{CH}_4,\text{out}}(\text{molmin}^{-1})}{F_{\text{Ne}}(\text{molmin}^{-1})} \right)}{\left(\frac{F_{\text{CH}_4,\text{in}}(\text{molmin}^{-1})}{F_{\text{Ne}}(\text{molmin}^{-1})} \right)}$$

3. Results and discussion

3.1. Catalyst Activity

The activities of the catalysts prepared using ZSM-5, mordenite and beta zeolites with different $\text{SiO}_2:\text{Al}_2\text{O}_3$ ratios were tested for

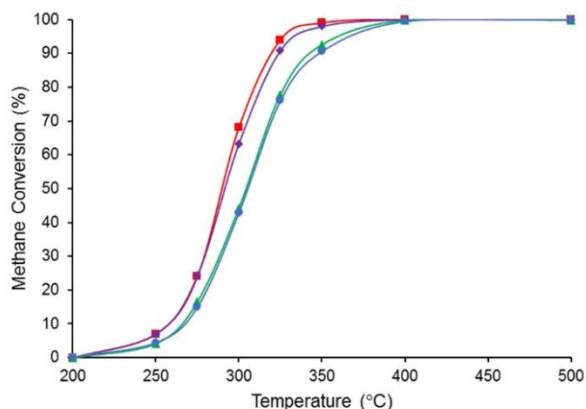


Figure 1. Catalytic activity profiles for methane oxidation over catalysts prepared on H-ZSM-5 supports with different $\text{SiO}_2:\text{Al}_2\text{O}_3$ ratios: Pd,Pt,TiO₂/H-ZSM-5 (23) (●), Pd,Pt,TiO₂/H-ZSM-5 (30) (▲), Pd,Pt,TiO₂/H-ZSM-5 (50) (◆), Pd,Pt,TiO₂/H-ZSM-5 (80) (■). Nominal composition: 5 wt.% Pd, 2 wt.% Pt, 17.5 wt.% TiO₂ on 75.5 wt.% zeolite.

methane combustion. The only products observed by GC analysis of the outlet stream of the reactor were CO₂ and H₂O and a carbon balance higher than 99% was obtained.

The activity profiles for the catalysts prepared using ZSM-5 supports are shown in Figure 1 and the data summarised in Table 1. The catalysts prepared from the ZSM-5 supports were all active for total methane oxidation and all achieved complete conversion at 400 °C. The Pd,Pt,TiO₂/H-ZSM-5 (23) catalyst showed the lowest activity of the catalysts tested with a temperature for 50% conversion ($T_{50\%}$) of 306 °C. However the activity of the catalysts increased with increasing $\text{SiO}_2:\text{Al}_2\text{O}_3$ ratio in the support, with the $T_{50\%}$ decreasing to 304 °C and 292 °C for the Pd,Pt,TiO₂/H-ZSM-5 (30) and (50) catalysts respectively and Pd,Pt,TiO₂/H-ZSM-5 (80) showed the highest activity of the H-ZSM-5 supported catalysts, with a $T_{50\%}$ of 290 °C and complete conversion around 350 °C. These differences are clearly seen when considering the conversion obtained at 300 °C being 43, 45, 63 and 68% for the Pd,Pt,TiO₂/H-ZSM-5 (23), (30), (50) and (80) catalysts, respectively.

The activity profiles for the catalysts prepared from the mordenite and beta zeolite topologies are compared with the Pd,Pt,TiO₂/H-ZSM-5 (30) catalyst in Figure 2 and the data summarised in Table 1. Comparison of the three zeolite topologies tested shows the mordenite to be the most active, followed by the beta and the ZSM-5 with $T_{50\%}$ of 289 °C, 298 °C and 304 °C respectively. It has been assumed that the small difference in the $\text{SiO}_2:\text{Al}_2\text{O}_3$ ratios of the catalysts shown here, similar to the Pd,Pt,TiO₂/H-ZSM-5 (23) and Pd,Pt,TiO₂/H-ZSM-5 (30) catalysts shown in Figure 1, is not responsible for the differences in the activity observed. To further understand the role of acidity and the location of the metals on the activity of

Table 1. The temperature required to reach 10% ($T_{10\%}$), 50% ($T_{50\%}$) and 90% ($T_{90\%}$) conversion for the combustion of methane using catalysts prepared on different zeolite supports.

Catalyst	$T_{10\%}$ (°C)	$T_{50\%}$ (°C)	$T_{90\%}$ (°C)
Pd,Pt,TiO ₂ /H-ZSM-5 (23)	268	306	348
Pd,Pt,TiO ₂ /H-ZSM-5 (30)	266	304	342
Pd,Pt,TiO ₂ /H-ZSM-5 (50)	258	292	324
Pd,Pt,TiO ₂ /H-ZSM-5 (80)	258	290	319
Pd,Pt,TiO ₂ /H-MOR (20)	257	289	314
Pd,Pt,TiO ₂ /H-BEA (38)	264	298	334

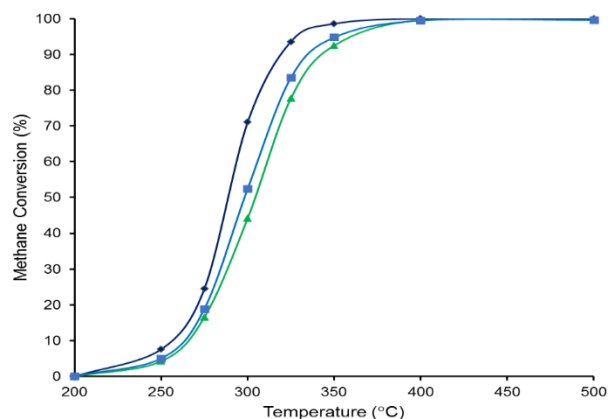


Figure 2. Catalytic activity profiles for methane oxidation over catalysts prepared on different supports Pd,Pt,TiO₂/H-ZSM-5 (30) (▲), Pd,Pt,TiO₂/H-MOR (20) (◆), and Pd,Pt,TiO₂/H-BEA (38) (■). Nominal composition: 5 wt.% Pd, 2 wt.% Pt, 17.5 wt.% TiO₂ on 75.5 wt.% zeolite.

the catalysts, a range of characterisation techniques were used.

3.2. Catalyst characterization

3.2.1. Physical Properties

The surface areas and pore volumes of the catalysts as determined by BET analysis²⁰ as well as the loading of palladium and platinum as determined by ICP-AES are summarized in Table 2. The measured surface areas of the supports (entries 1-4) are consistent with those provided by Alfa Aesar.²⁴ As expected, the surface area of the zeolite decreased from between 413 and 432 m^2g^{-1} to 312 and 337 m^2g^{-1} and similarly the micropore volume decreased from between 0.11 and 0.13 cm^3g^{-1} to 0.07 and 0.08 cm^3g^{-1} on addition of Pd, Pt and TiO₂ (entries 6-9). The metal loading as measured by ICP-AES was found to be similar to the desired loading, being between 5.3 and 5.4 and 2.2 and 2.7 wt.%, for Pd and Pt respectively. Values shown in entries 6-9 show only a slight variation in surface area, pore volume and metal loading among the four catalysts meaning differences in activity are unlikely to be attributed to these properties.

Table 2. Surface areas, micropore volumes and Pd and Pt loadings of the supports and catalysts

Entry	Sample	BET surface area (m^2g^{-1}) ^a	Micropore volume (cm^3g^{-1}) ^b	Pd wt. % ^c	Pt wt. % ^c
1	ZSM-5 (23)	413	0.11	-	-
2	ZSM-5 (30)	426	0.11	-	-
3	ZSM-5 (50)	432	0.12	-	-
4	ZSM-5 (80)	430	0.13	-	-
5	TiO ₂ (anatase)	45	-	-	-
6	Pd,Pt,TiO ₂ /H-ZSM-5 (23)	312	0.08	5.4	2.7
7	Pd,Pt,TiO ₂ /H-ZSM-5 (30)	317	0.07	5.4	2.6
8	Pd,Pt,TiO ₂ /H-ZSM-5 (50)	337	0.08	5.3	2.6
9	Pd,Pt,TiO ₂ /H-ZSM-5 (80)	330	0.07	5.3	2.2
10 ^d	Aged Pd,Pt,TiO ₂ /H-ZSM-5 (80)	317	0.07	-	-

^aestimated using the BET model with criteria proposed by Rouquerol *et al.*²⁰ and described in ESI 1. ^bcalculated using t-plot method ^cdetermined using ICP-AES. ^dafter 50 h on stream at 300 °C

3.2.2 NH₃-TPD

The surface acidity of the zeolite supports and corresponding catalysts were studied by NH₃-TPD and the results for Pd,Pt,TiO₂/H-ZSM-5 (23) are illustrated in Figure 3 with the other catalysts shown in ESI 2. The results are as expected with two broad peaks observed for the zeolite supports at low temperature (LT - below 300 °C) and high temperature (HT - above 300 °C). The LT peak can be deconvoluted into two components; component 1 (blue) at 150 °C which is attributed to the NH₃ bound via hydrogen bonding to an NH₄⁺ ion formed by NH₃ and Brønsted acid sites and component 2 (green) at 200 °C, which is attributed to the weakly bound NH₃ to weak Lewis acid sites [25]. On the other hand, the HT peak can be fitted using only one component, component 5 (purple) at ca. 380 °C, which corresponds to NH₃ desorbed from the strong Brønsted acid sites.^{25, 26}

Compared to the supports alone, two extra components were found in the TPD profile of the catalysts, namely component 3 (light blue) at ca. 240 °C and 4 (orange) at around 340 °C (Figure 3). The surface acidity of Pd/TiO₂ catalysts was studied by Gonzalez *et al.*, and a desorption peak was found at around 238 °C in the NH₃-TPD profiles of these samples.²⁷ Lou *et al.* employed pyridine Fourier-transform infrared spectroscopy (FT-IR) to study Pd/H-ZSM-5 materials and subsequently assigned a peak at ca. 300 °C to strong Lewis acid sites derived from the coordinatively unsaturated Pd atoms, which, in turn, are the products from the interaction between the highly dispersed PdO_x and the Brønsted acid sites on the surface of ZSM-5.¹⁰ TiO₂ in the anatase form was shown to possess a certain degree of acidity. However this is not thought to contribute strongly to the profile as the amount of acid sites in anatase TiO₂ is small (0.042 mmol per gram of TiO₂) compared to the values of components 3 and 4 shown in Table 3 (mmol per gram of the catalysts) and the temperature of desorption is also lower (around 200 °C)^{28,29}. Therefore, the components 3 and 4 have been assigned to the NH₃ bound to PdO_x/PtO_x species dispersed on TiO₂ and H-ZSM-5 media.

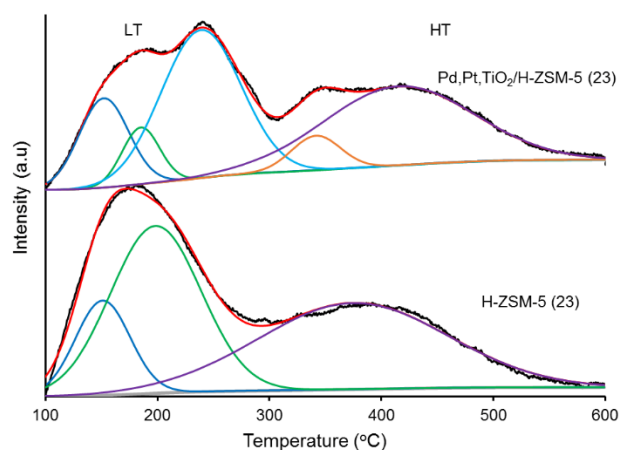


Figure 3. NH₃-TPD profiles of H-ZSM-5 (23) and the corresponding Pd,Pt,TiO₂/H-ZSM-5 (23) catalyst. Colour codes: signal (black), fit (red), background (grey), and components 1-5 (blue, green, light blue, orange and purple, respectively).

Table 3. Quantification of different acid sites based on NH₃-TPD analysis

Samples	Com. 1 ¹	Com. 2	Com. 3	Com. 4	Com. 5	Total ²
H-ZSM-5(23)	0.16	0.47	-	-	0.51	1.14
H-ZSM-5(30)	0.09	0.42	-	-	0.38	0.89
H-ZSM-5(50)	0.05	0.25	-	-	0.25	0.54
H-ZSM-5(80)	0.04	0.19	-	-	0.21	0.44
Pd,Pt,TiO ₂ /H-ZSM-5(23)	0.14	0.07	0.36	0.05	0.37	0.98
Pd,Pt,TiO ₂ /H-ZSM-5(30)	0.07	0.22	0.13	0.14	0.14	0.70
Pd,Pt,TiO ₂ /H-ZSM-5(50)	0.15	0.23	0.16	0.09	0.03	0.66
Pd,Pt,TiO ₂ /H-ZSM-5(80)	0.06	0.15	0.06	0.16	0.03	0.46

¹amount of NH₃ desorbed corresponding to current component, in mmol g⁻¹ ²total amount of NH₃ desorbed by the sample, in mmol g⁻¹

Quantitatively, the amount of desorbed NH₃ listed in Table 3 shows the decrease in the number of stronger Brønsted acid sites (component 5) as the SiO₂:Al₂O₃ ratio increases in both the unfunctionalized supports and in the supported catalysts. With the same SiO₂:Al₂O₃ ratio, there is quite a significant decrease in the number of Lewis acid sites (component 2) and Brønsted acid sites (component 5) in the catalysts compared to the unfunctionalized supports. The same phenomena were observed in the work of Lou *et al.* and these decreases were later assigned to the removal of extra-framework aluminium and the occupancy of Brønsted acid sites by the basic PdO_x species, respectively.¹⁰

As can be seen in Table 1 and Table 3, the Pd,Pt,TiO₂/H-ZSM-5 (80) catalyst which contains the least number of acid sites led to the highest catalytic activity implying that the acidity of the catalysts does not reflect the observed catalytic activity and that the importance of acid sites in direct methane activation is not observed in the current work.

3.2.3. XRD analysis

XRD diffractograms for H-ZSM-5(80), Pd,Pt,TiO₂/H-ZSM-5 (80), 2%Pt/TiO₂/H-ZSM-5 (80), 5%Pd/TiO₂/H-ZSM-5 (80), and the titania anatase component are shown in Figure 4.

Comparison of the diffractograms shown in Figure 4 shows that the zeolite support retains its crystallinity after the addition of the metallic components. The first two diffraction peaks in the catalysts and their supports at 2θ between 8 ° and 10 ° can be assigned to the (101) and (011) planes of the MFI (ZSM-5) phase, respectively.¹⁰

Diffraction peaks corresponding to crystalline PdO and to TiO₂ in the anatase polymorph were determined and are marked, in Figure 4e.^{30,31} While no peak corresponding to PtO₂ is observed in Figure 4e, it is not possible to rule out the presence of PtO, since the reflections overlap with those of PdO because of their similar position.^{30,32}

An additional reflection was detected at 2θ ~ 40 °, which is not present in the diffractogram of 5 % Pd/TiO₂/H-ZSM-5 (80), the sample without Pt (Figure 4d). This reflection was observed in

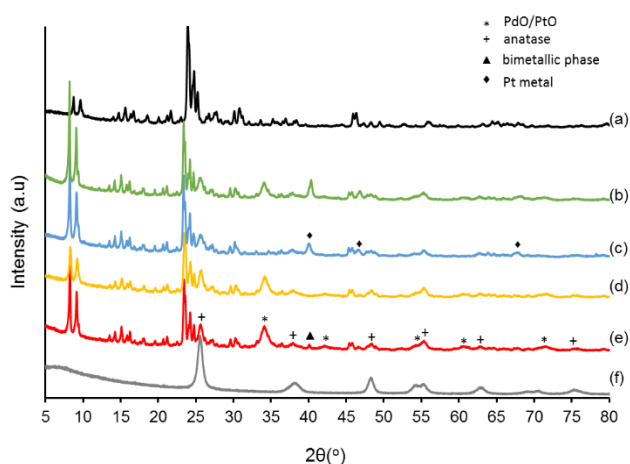


Figure 4. XRD diffractograms of the H-ZSM-5 (80) supported catalysts with ZSM-5 and TiO₂ for reference. (a) H-ZSM-5 (80), (b) Pd,Pt,TiO₂/H-ZSM-5 (80) H₂ pretreated, (c) 2%Pt,TiO₂/H-ZSM-5 (80), (d) 5%Pd,TiO₂/H-ZSM-5 (80), (e) Pd,Pt,TiO₂/H-ZSM-5 (80) and (f) TiO₂ (anatase). All catalysts contain 17.5 wt.% TiO₂ and 5 wt.% Pd and 2wt.% Pt where not stated.

each of the Pd,Pt,TiO₂/H-ZSM-5 (80) catalysts and became more prominent in the H₂ pretreated sample (Figure 4b), which confirms its metallic nature. This peak has previously been assigned to the 111 reflection of an alloy between Pd and Pt, although due to the similarity of the unit cells of the Pd and Pt metallic phases, it is not a definitive proof for the existence of a bimetallic phase.^{30, 33, 34} However, given its absence from the diffractograms of the monometallic Pd catalyst, from now on, this phase is referred to as the bimetallic phase of Pd and Pt.

The particle size of the PdO, TiO₂ and bimetallic components calculated from the XRD data using the Scherrer equation are given in Table 4. It can be seen that there is little variation observed in the crystallite size of PdO, TiO₂ and the bimetallic phase from one sample to another, especially taking into account the limit in accuracy of the analysis.³⁵ The only exception is the case of the Pd,Pt,TiO₂/H-MOR (20) sample, in which the average crystallite size of the bimetallic phase is significantly smaller than those of the other samples. The similarity in particle size of PdO obtained with H-ZSM-5 supports of different SiO₂:Al₂O₃ ratios will be later confirmed using STEM-EDS, TEM and EXAFS analysis.

The ratio of the bimetallic phase peak to the PdO peak was taken as a measure of the proportion of the bimetallic species that was present compared with the metal oxide (PdO or PtO). Table 4 shows that for the catalysts prepared using the MFI zeolite, this metal:oxide ratio increases with increasing SiO₂:Al₂O₃ ratio, in line with the increasing activity of these catalysts. To determine if this was also applicable to other zeolite structures, a similar analysis was carried out with the catalysts prepared using the mordenite and beta supports. Figure 5 shows that there is a correlation between the ratio of the amount of bimetallic phase compared to the amount of PdO and the activity of the catalysts, with catalysts containing a higher proportion of the bimetallic phase and a lower proportion of oxide being the more active.

Table 4. Summary of crystallite sizes for PdO, TiO₂ and bimetallic phases and relative peak areas determined by XRD.

Catalyst	Average crystallite size (nm)*			Bimetallic /PdO peak area ratio**
	PdO	TiO ₂	Bimetallic	
Pd,Pt,TiO ₂ /H-ZSM-5(23)	5.7	13.2	39.9	0.024
Pd,Pt,TiO ₂ /H-ZSM-5(30)	6.8	12.7	39.4	0.032
Pd,Pt,TiO ₂ /H-ZSM-5(50)	6.9	11.0	36.8	0.051
Pd,Pt,TiO ₂ /H-ZSM-5(80)	7.6	12.5	38.1	0.062
Pd,Pt,TiO ₂ /H-MOR(20)	7.0	12.6	28.2	0.064
Pd,Pt,TiO ₂ /H-BEA(38)	7.0	12.7	40.3	0.038

* calculated using Scherrer equation applying to the PdO (101) peak at ~34 °, the TiO₂ (101) peak at ~25 °, and the bimetallic peak at ~40 °; the peak width at half-height was determined by fitting the experimental data using the program Highscore Plus. ** the ratio of the peak area between the bimetallic peak at 40 ° and PdO (101) at ~34 °.

3.2.4. STEM and electron tomography

To further study the particle size of the crystallites and to confirm the location of the different metals, the catalysts were characterised using STEM-HAADF and STEM-EDS.

High-resolution HAADF-STEM images (Figure 6) reveal the structure of the catalyst. Nanoparticles rich in Pd/Pt stand out as bright spots due to their significantly higher atomic number compared with those of the other components. Anatase (100) and ZSM-5 were also clearly identified based on their observed lattice spacings and crystal structures.

The particle size distribution of Pd/Pt rich nanoparticles was measured from the HAADF-STEM images and is shown in Figures 6c and 6f. The presence of the oxide support makes it difficult to distinguish crystallographic information in these particles, and therefore the distributions shown here represent

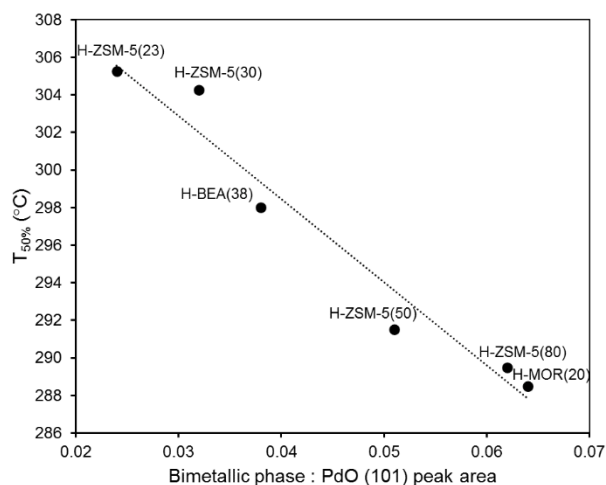


Figure 5. Correlation between the ratio of the peak area for the peak associated with the bimetallic phase (at ~40 °) to the peak associated with PdO (at ~34 °), against the activity of the catalyst as given by T_{50%}. Each point is labelled with the name of the zeolite support.

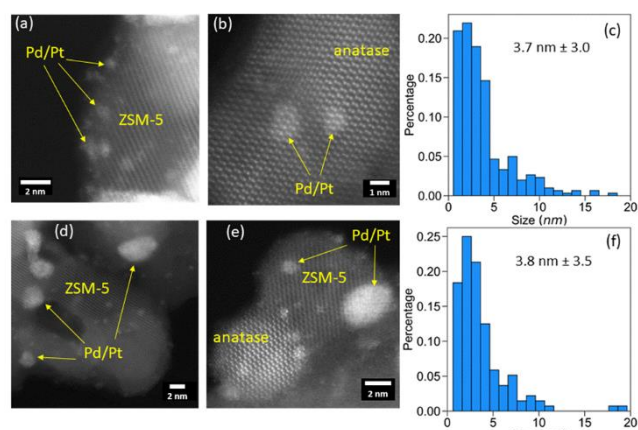


Figure 6. High-resolution STEM-HAADF images and Pd/Pt particle size distribution charts for Pd/Pt/TiO₂/H-ZSM-5 (23) (a, b and c) and Pd/Pt/TiO₂/H-ZSM-5 (80) (d, e and f).

both Pd and Pt rich particles (identified as such from the relatively high scattering cross section of these two metals). Average particle sizes of 3.7 ± 3.0 nm and 3.8 ± 3.5 nm are found for the Pd,Pt,TiO₂/H-ZSM-5 (23) and Pd,Pt,TiO₂/H-ZSM-5 (80) catalysts, respectively showing a negligible difference in particle size of Pd/Pt on the two supports. Comparison with the XRD Scherrer analysis suggests that these particles are likely to be PdO and PtO. Thus, the noticeable difference in catalytic activity between Pd/Pt/TiO₂/H-ZSM-5 (23) and Pd/Pt/TiO₂/H-ZSM-5 (80) shown in Figure 1 is unlikely to result from the difference in the Pd/Pt dispersion found in the two catalysts. STEM-HAADF and the corresponding STEM-EDS elemental maps of Pd,Pt,TiO₂/HZSM-5 (23) and Pd,Pt,TiO₂/HZSM-5 (80) catalysts are shown in Figures 7(a-h). The brighter contrast in the STEM-HAADF images is confirmed to correspond to areas rich in Pd and Pt (Figures 7a and 7e), while the TiO₂ and ZSM-5 support areas have weaker HAADF intensity and produce the expected Ti and O or Si and O X-ray counts respectively (see ESI Figures S3 and S4). The STEM-EDS data demonstrates the presence of highly dispersed Pd and Pt rich particles in the catalyst which are mostly co-located revealing an intimate mixing of Pd and Pt (Figures 7b-d, 7f-h, and 7j-l). Comparison of the Ti and Si STEM-EDS elemental maps allows the zeolite and anatase support particles to be clearly separated (Figure S3 and S4). Figure S3 shows that TiO₂ was deposited around the outside of the zeolite support and the TiO₂ particle size is consistent with the average crystallite size of 13 nm measured by XRD (Table 4), which is much larger than the ZSM-5 pore size (~ 0.5 nm). The Pd and Pt nanoparticles were found to be deposited on both ZSM-5 and TiO₂, as well as at the interface between the two materials, (Figure S3 and Figure S4). However, careful inspection of 15 regions of the Pd/Pt/TiO₂/HZSM-5 (23) and Pd/Pt/TiO₂/HZSM-5 (80) catalysts revealed a slight preference for the metal catalyst to be associated with the TiO₂ rather than the zeolite; 47 % of the regions studied had Pd/Pt preferentially located on the TiO₂ particles, while the metals were equally distributed for 40 % of the regions, and preferentially located on the zeolite in 13 % of regions.

This is perhaps surprising given the higher surface area of zeolite available, but may be due to the difference in the point of zero charge between TiO₂ and ZSM-5 (anatase TiO₂ is reported to be 4.2^{36} while H-ZSM-5 with a SiO₂:Al₂O₃ ratio of 30 is reported to be 5.0^{37}). The nanoparticle location and morphology of the catalysts was further studied using STEM-HAADF electron tomography, Figure 8. Figure 8a shows surface-rendered representations of the segmented reconstructed volume of Pd,Pt,TiO₂/H-ZSM-5 (23). Here, the small red volumes, correspond to the high intensity areas of the HAADF images, that is, to the Pd/Pt rich nanoparticles; while the region in blue corresponds to a TiO₂ support particle. A key feature which can be extracted from the 3D tomographic data in Figure 8a, is the location of the Pd/Pt nanoparticles on the TiO₂. 2D slices through the 3D reconstructed volume shown in Figures 8d-8f reveals the porous structure of the TiO₂ support and the location of Pd/Pt nanoparticles inside and on the surface. The majority of the Pd/Pt particles were found on the external surface of TiO₂, but, there are also some particles (2 out of total 15 particles) located inside the TiO₂ support. It was observed that some pores in the TiO₂ are not connected to the outer surface, and hence nanoparticles that are located on these surfaces are not likely to be involved in the catalytic reaction. A second tomographic data set for Pd/Pt/TiO₂/H-ZSM-5 (23) in which all components (Pd/Pt nanoparticles, TiO₂ and zeolite) are visible is shown in ESI 4 (Figure S5). Again, the majority of Pd/Pt particles are located on the external surface of the TiO₂ and, additionally, the TiO₂ particles were found on the external surface of the zeolite (consistent with the 2D STEM-EDS data in Figure S3). However, it is worth noting that these tomographic data sets have a voxel resolution of ~ 0.5 nm, so it is not possible to detect the smallest nanoparticles, <0.5 nm, which may be located inside the pores of ZSM-5. A similar reconstruction for high SiO₂:Al₂O₃ ratio sample Pd,Pt,TiO₂/H-ZSM-5 (80) is shown in ESI 4 (Figure S6) demonstrating that the size distributions and location of the Pd/Pt nanoparticles was found to be similar in the two samples despite their different SiO₂:Al₂O₃ ratios.

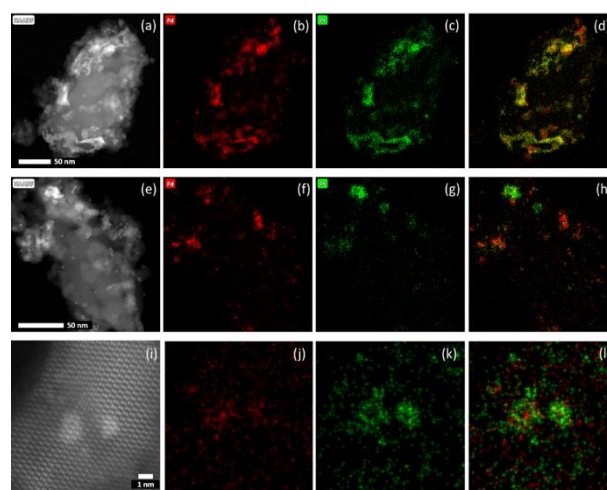


Figure 7. STEM HAADF images (left hand column), individual Pd (red) and Pt (green) EDS elemental maps and composite Pd+Pt overlay image (where red and green combine to yellow). (a-d) and (i-l) are the Pd,Pt,TiO₂/H-ZSM-5 (23) sample, (e-h) is the Pd,Pt,TiO₂/ZSM-5 (80) catalyst. The red indicates Pd and the green Pt elements with the yellow indicating areas where Pd and Pt are co-located.

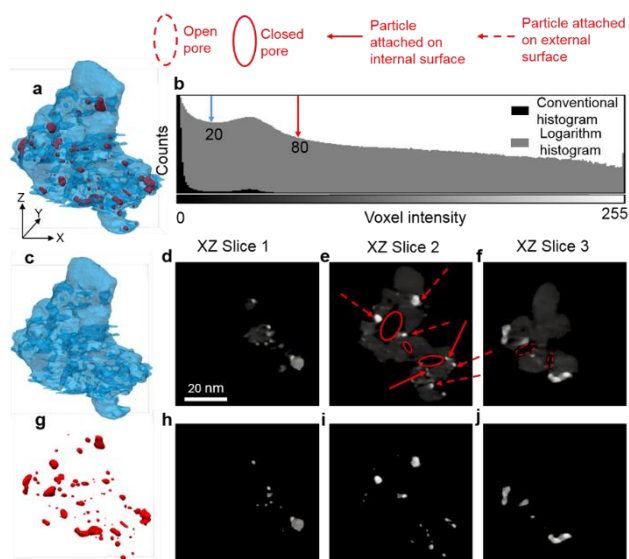


Figure 8. 3D visualisation and 2D orthoslices from STEM-HAADF electron tomography reconstruction of the Pd,Pt,TiO₂/H-ZSM-5 (23) catalyst a) 3D surface render of the reconstruction with colours indicating intensity differences, blue, low HAADF intensity (TiO₂ particle), red, high HAADF intensity (Pd and Pt rich particle). b) histogram of the unprocessed reconstruction. Voxel intensities ranging from 20-255 are rendered blue (TiO₂ support, shown in c) while intensities of 80-255 are rendered red (Pd and Pt rich particles, shown in g). d-f) and h-j) are 2D slices extracted from c) and g) respectively. Legend above refers to the annotations in e and f.

3.2.5. XAS

The XANES spectra of the three catalysts, Pd,Pt,TiO₂/HZSM-5 (23, 50, 80) and the reference materials PdO, PtO₂ and Pd, Pt metals at the Pd K-edge and the Pt L_{III}-edge are shown in Figure 9.

It can be immediately seen that the Pd XANES spectra of the catalysts are more similar to those of the corresponding oxide, PdO, rather than that of the metal, Pd foil, indicating that the Pd is present predominantly as oxides. Furthermore, looking closely at both the position of the adsorption edge and intensity of the “white line” peak indicates the average oxidation state of Pd in the three catalysts as being significantly higher than that of the Pd foil reference. The slight shift in the edge position and the slight increase in the intensity of the “white line” peak in the Pd,Pt,TiO₂/H-ZSM-5 (23, 50, 80) samples compared to those of the PdO reference suggests that the samples consist of PdO but that the local Pd environment is not the same as the reference. At the Pt L_{III}-edge, by comparing the intensity of the “white line” peaks, the average oxidation state of Pt is estimated to be between those of PtO₂ and Pt foil references (Figure 9b). Moreover, there is hardly any difference in the oxidation states of Pd and Pt supported on H-ZSM-5 with different SiO₂:Al₂O₃ ratios.

Figure 10 shows the EXAFS measured at the Pd K-edge of the three catalysts and for PdO and Pd foil as references. In agreement with the XANES results, EXAFS data shows the similarities between the spectra for the three catalysts with that of the PdO reference. Specifically, there are two main peaks that can be observed in the Fourier transform spectra in R-space

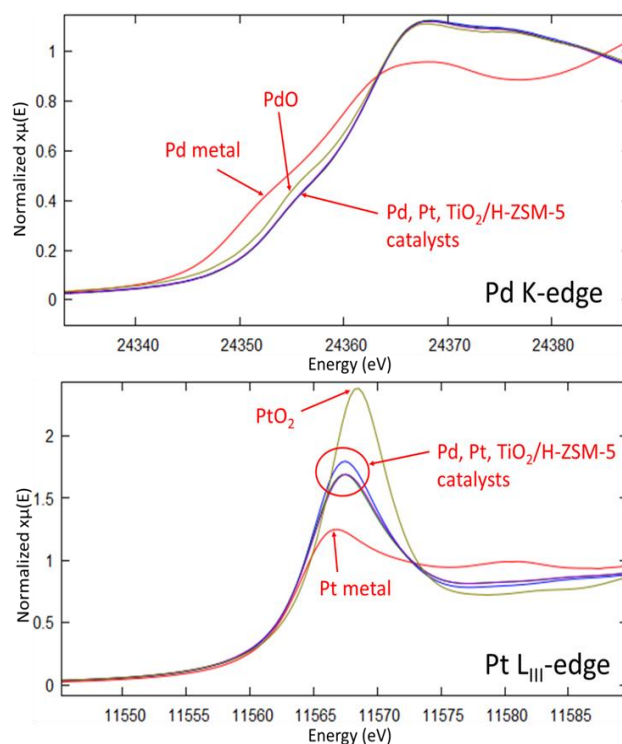


Figure 9. XANES at the Pd K-edge and the Pt L_{III}-edge of the three catalysts Pd,Pt,TiO₂/H-ZSM-5 (23 (blue), 50 (purple), 80 (green)) and PdO (yellow), PtO₂ (yellow) and Pd (red) and Pt metal (red) references.

of the three catalysts and PdO reference. The first peak presents at an uncorrected distance of 1.6 Å, which corresponds to the first Pd-O shell. The second peak, spanning between 2.1 and 3.5 Å, is a combination of the contributions from the second and third Pd-Pd shells. To obtain more detailed structural information, a theoretical model of tetragonal PdO was used to

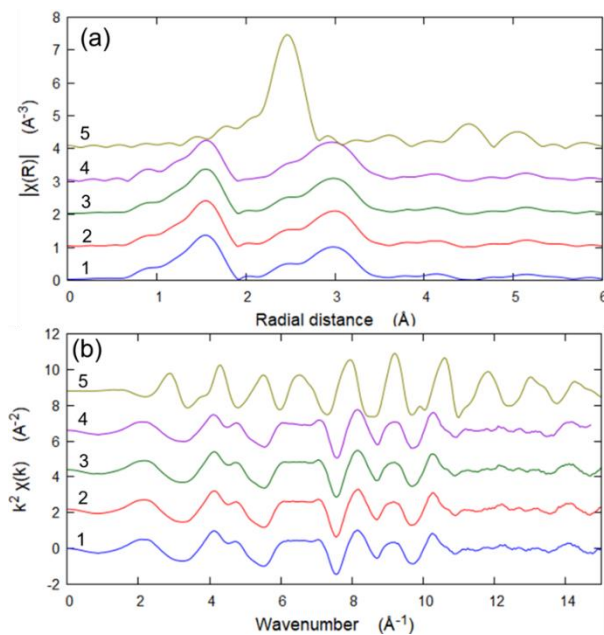


Figure 10. k³-weighted Pd K-edge EXAFS spectra for the three catalysts and PdO, Pd metal references; (a) R-space; (b) k-space. 1-3: Pd,Pt,TiO₂/H-ZSM-5 (23, 50, 80); 4: PdO; 5: Pd metal.

fit the experimental data. The PdO reference was analysed first to verify the reliability of the model, of which the best-fit parameters and the fit in R-space are shown in Table S1 and Figure S7 of ESI 5, respectively. The data shown in Table S1, specifically the coordination numbers (CNs) of the two Pd-Pd shells, indicates similar PdO particle size in the three catalysts. This supports the conclusions drawn from the XRD and TEM analysis, and suggests that broadly speaking, there are no major differences in Pd composition and physical characteristics between the samples. The relatively large value of CNs of Pd-Pd shells obtained from the catalysts suggests that PdO presents dominantly as aggregates/nanoparticles. The theoretical ion exchange capacity between protons in H-ZSM-5 with SiO₂:Al₂O₃ ratios of 23, 50 and 80 and Pd²⁺ can be calculated as 6.7, 3.3 and 2.1 (in Pd wt.%), respectively. Taking into account the actual concentrations of Pd of 5.3 wt.% in the catalysts, the fact that Pd exists mostly as aggregates/NPs, even with H-ZSM-5 (23) as support, suggests that either the palladium precursor molecules could not diffuse inside ZSM-5 pores or that ion exchanged Pd species sintered upon heat treatment and formed PdO aggregates. In addition, the coordination number and bond distance of the Pd-O shell determined by the curve-fitting analysis were independent of the SiO₂:Al₂O₃ ratio of H-ZSM-5 and are similar to those of bulk PdO. This confirms the observations made in the XANES that the local structure of dispersed PdO is similar to that of bulk PdO.

EXAFS spectra measured at the platinum edge of the three catalysts, PtO₂ and Pt foil references are shown Figure 11.

The spectra of the three catalysts show a closer resemblance to that of the PtO₂ reference compared to that of Pt foil, which suggests the oxide nature of Pt in those samples. However, there are a few differences between the spectra of the catalysts and that of the PtO₂ reference (Figure 11a). This is likely because

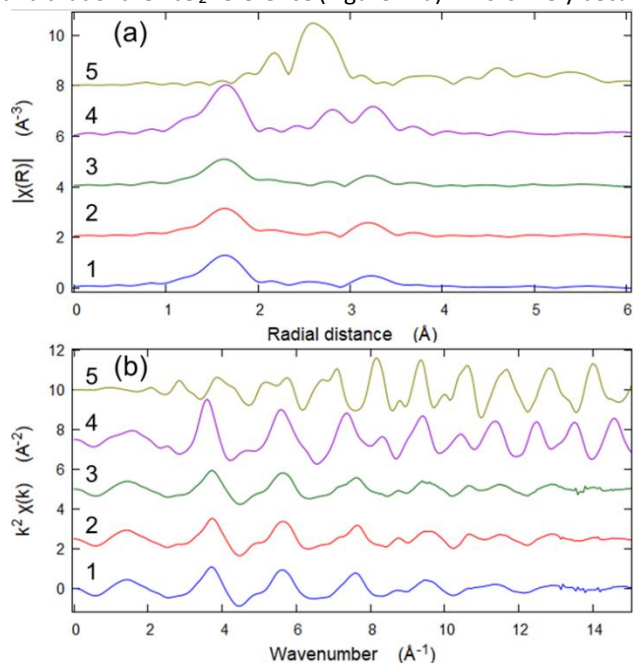


Figure 11. k^3 -weighted Pt L_{III} -edge EXAFS spectra for the three catalysts and PtO₂, Pt metal references; (a): R-space; (b): k-space; 1-3: Pd,Pt,TiO₂/H-ZSM-5 (23, 50, 80); 4: PtO₂; 5: Pt metal.

Pt is present in the catalyst as PtO_x with $x < 2$, consistent with the XANES result (Figure 9).

The theoretical model of tetragonal PtO was also used to fit the experimental data from Pd,Pt,TiO₂/H-ZSM-5 (23) (Figure S8) as PtO is the only available model of PtO_x with $x < 2$. The best-fit parameters of such a fit are summarized in Table S2. As can be seen in Table S2, the CNs obtained with the two Pt-Pt shells are much smaller than those of the crystallographic model of PtO. This indicates a key difference compared to what was previously observed at the Pd edge and suggests that the major part of Pt presents as small clusters and ions. The same model was used to fit the experimental data from Pd,Pt,TiO₂/H-ZSM-5 (50 and 80) catalysts but did not result in good fits. It can be seen in Figure 11a that the three catalysts share the two highest peaks at uncorrected distances of 1.6 Å and 3.2 Å although they possess minor differences in the peaks between 2 and 3 Å. These minor peaks likely arise because of the interaction between PtO and the TiO₂ and H-ZSM-5 supports, and as such this could cause the subtle differences in speciation and location of Pt in the catalysts compared to the model of pure PtO. The fact that this misfit was only observed at the Pt edge might be due to the higher degree of PtO-support interaction, which is in turn is likely to be the consequence of the higher dispersion of PtO compared to that of PdO.

3.2.6. XPS

To further study the oxidation state of Pd and Pt species of Pd,Pt,TiO₂/H-ZSM-5 catalysts, X-ray photoelectron spectroscopy (XPS) was conducted as shown in Figure 12. As can be seen in Figure 12a, Pd mostly presents as Pd²⁺(PdO) with a binding energy of ca. 337 eV.³⁸ Peak fitting also reveals peaks corresponding to Pd²⁺ satellites³⁹ and to the core-level spectrum of Pt 4d_{3/2} at ca. 331.7 eV.⁴⁰ A minor contribution from Pd⁰ (metal) at a binding energy of 335 eV⁴¹ was found in Pd,Pt,TiO₂/H-ZSM-5 (80) (Figure 12a). Here, the ratio of the 3d_{5/2} peak areas corresponding to Pd⁰ and Pd²⁺ were calculated to be almost 0.01, which is significantly smaller than the respective ratio shown in Table 4 (0.062). This is expected since XPS analysis is only sensitive to chemistry of the surface, where oxides are likely to dominate, while the XRD result represents an average of the whole sample. Although there is some evidence for the presence of Pd⁰ in the Pd,Pt,TiO₂/H-ZSM-5 (50) catalyst, a reliable estimation of the amount is not possible, while it is not viable to include any contribution from metallic Pd to the experimental data for Pd,Pt,TiO₂/H-ZSM-5 (23). Figure 12b shows Pt to predominantly present as Pt²⁺ with a binding energy of approximately 72.0 eV and with a minor contribution from Pt⁴⁺ represented by a peak at ca. 74.0 eV⁴² supporting the findings from XANES and EXAFS. Moreover, both Pd 3d_{5/2} and Pt 4f_{5/2} peaks were shown to shift to lower binding energies of 336.68 eV from 337.18 eV for Pd and 75.18 eV from 75.58 eV for Pt as the SiO₂:Al₂O₃ ratio increased from 23 to 80 (Table S3 in ESI 6). This indicates a decrease in electron deficiency of Pd and Pt on the less acidic supports, which agrees well with literature.^{43, 44} These findings support the results from XRD analysis, specifically the bimetallic/PdO ratio listed in

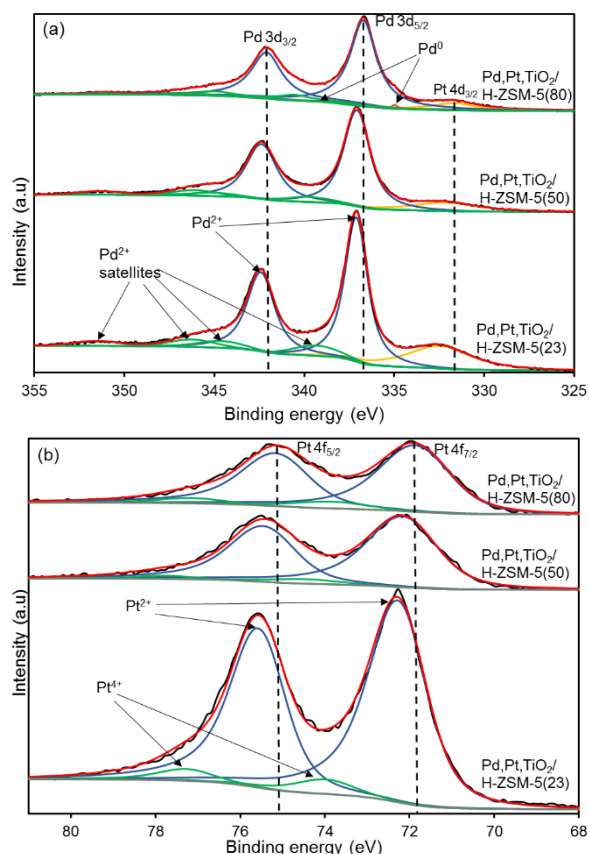


Figure 12. XPS spectra of Pd,Pt,TiO₂/H-ZSM-5 catalysts in (a) Pd 3d and (b) Pt 4f regions. Colour codes: signal (black), fit (red), background (grey), Pd²⁺ (blue), Pd²⁺ satellites (green), Pd⁰ (orange), Pt 4d_{3/2} (yellow), Pt²⁺ (blue), Pt⁴⁺ (green).

Table 4, which indicates the higher quantity of metallic species being present in the ZSM-5 supported catalysts of higher SiO₂:Al₂O₃ ratios. Interestingly, Pd,Pt,TiO₂/H-ZSM-5 (80 and 50) are also the more active catalysts compared to the Pd,Pt,TiO₂/H-ZSM-5 (30 and 23) catalysts (Table 1) suggesting the importance of a lower oxidation state or facile redox behaviour for higher activity. Khudorozhkov et al. also used in-situ XPS to show the presence of Pd²⁺ and Pd(0) on working Pd/Al₂O₃ catalysts for propane oxidation.⁴⁵

3.2.7. TPR

TPR profiles of the catalysts supported on H-ZSM-5 materials of different SiO₂:Al₂O₃ ratios are shown in Figure 13. Figure 13a shows that relatively sharp peaks with high intensity were observed at -5.8, -3.9, -8.7 and -3.5 °C for the catalysts corresponding to SiO₂:Al₂O₃ ratios of 23, 30, 50, and 80, respectively; which can be attributed to the reduction of Pd or Pt oxides to the corresponding metals.⁴⁶⁻⁴⁸ Although there is no correlation between the reduction temperature of the oxides and the SiO₂:Al₂O₃ ratio of the support, the area under the peaks is shown to decrease from 18.3, 17.5, 14.2 to 10.8 (in arbitrary area units calculated per gram of sample) with the increase in the SiO₂:Al₂O₃ from 23, 30, 50 to 80 respectively. This suggests either there is less oxide or the average oxidation state is lower in the catalysts with higher SiO₂:Al₂O₃ ratios. Figure 13b is the enlarged version of the profile of the Pd,Pt,TiO₂/H-ZSM-5

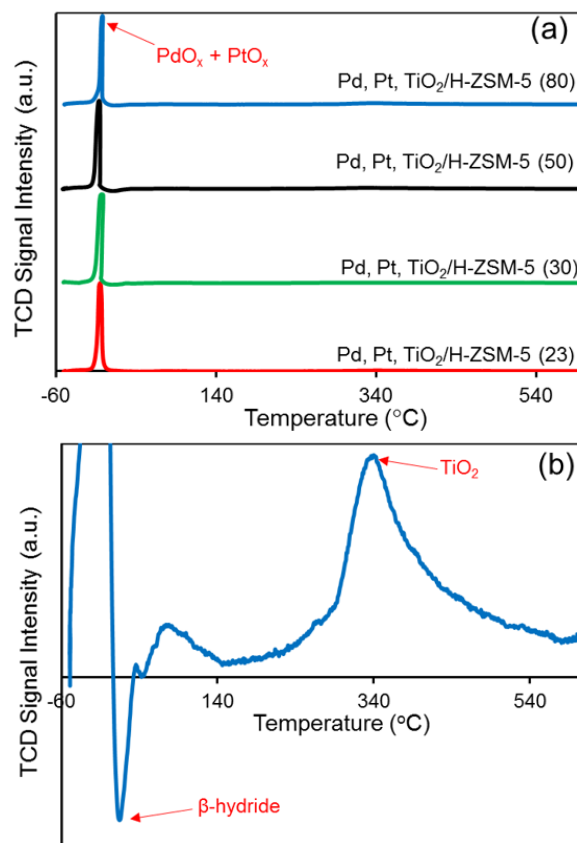


Figure 13. H₂-TPR profiles of (a) the four catalysts with different SiO₂:Al₂O₃ ratios in the support and (b) enlarged versions of the profile of Pd,Pt,TiO₂/H-ZSM-5 (80) to show the peaks corresponding to the presence of β -hydride and TiO₂ reduction.

(80) catalyst shown in Figure 13a. The negative peak, observed *ca.* 14 °C in the profiles of Pd,Pt,TiO₂/H-ZSM-5 (30, 50, 80) and around 44 °C in that of Pd,Pt,TiO₂/H-ZSM-5 (23), shows the release of H₂ and can be attributed to the decomposition of a β -hydride species of Pd (or Pt).⁴⁹ The intensity of this peak for Pd,Pt,TiO₂/H-ZSM-5 (30, 50, 80) is significantly higher than that of Pd,Pt,TiO₂/H-ZSM-5 (23), implying a larger quantity of the β -hydride species present. The second peak, observed between 240-540 °C, is quite broad and can be assigned to the reduction of TiO₂.¹⁹ The lower oxidation state of Pd, as signified by the decrease in peak area for PdO reduction and increase in peak area for decomposition of the β -hydride species, on zeolites with higher SiO₂:Al₂O₃ ratios suggests the possibility of an easier exchange between or co-existence of PdO and Pd(0) under reaction conditions for the more active catalysts. The suggestion of a positive effect of the presence of a metallic species or oxides with low oxidation states on catalyst activity is consistent with that found from XRD (Table 4) and XPS analyses (Figure 12a).

3.3 Catalyst stability

The stability of catalysts prepared using different supports was compared and illustrated in Figure 14. The catalyst prepared on H-ZSM-5 (23) was found to be the most stable while the other two lost around 13% (relatively) of their corresponding activities

over 35 h on stream at 300 °C. The better stability of the catalyst supported on H-ZSM-5 (23), may be explained by its higher

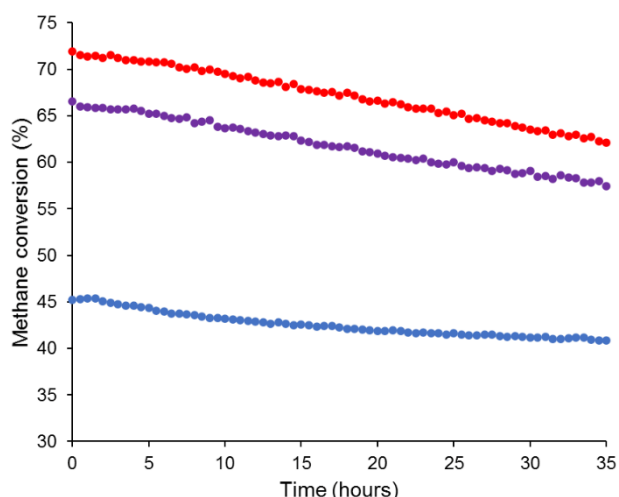


Figure 14. Comparison of the stability of catalysts prepared on different supports for reaction at 300 °C. Pd,Pt,TiO₂/H-ZSM-5 (23) (●), Pd,Pt,TiO₂/H-ZSM-5 (50) (●), Pd,Pt,TiO₂/H-ZSM-5 (80) (●).

acidity, Table 3, which has been reported to increase the stability of the PdOx species on the surface.¹⁵

To further understand the mechanism of deactivation, the Pd,Pt,TiO₂/H-ZSM-5 (80) catalyst that had been run for 50 h was recovered and analysed using XRD, BET, TGA-O₂ and STEM. XRD analyses, shown in Figure S9 in ESI 7, confirmed that the crystal structure of this sample remained intact after 50 h of reaction at 300 °C. Furthermore, BET analysis reveals that the surface area and micropore volume of Pd,Pt,TiO₂/H-ZSM-5 (80), before and after reaction, are almost identical (entries 9 and 10 in Table 2). TGA analyses of the two samples in O₂ was carried out and the result is illustrated in Figure S10 in ESI 7. It can be seen that by heating the two samples in O₂ flow from 50 to 800 °C the original and aged catalysts have lost approximately 5 and 3 % of their original weight, respectively. However, most of the above weight loss occurred around 100 °C and can be attributed to the desorption of the physisorbed water (moisture) in these samples. Thus, no sign of coke formation was observed here. Original and aged samples were also analysed by HAADF and STEM-EDS and an important difference was observed between the two samples. It can be seen in Figures S11 (b and c), Pd and Pt are finely dispersed and well mixed in the original sample. Whereas, a significant degree of aggregation has occurred in the deactivated sample as can be seen in Figures S11 (e and f). However, it is interesting to observe that Pd and Pt signals were still found in the same location before and after the course of aggregation, suggesting the presence of bimetallic species. XRD data shown in Figure S9 revealed that the average crystallite size of PdO has increased from 7.6 nm in the original catalyst to 10.4 nm in the aged one, which further confirms the aggregation shown in STEM analysis. The aggregation shown here might be one of the reasons for the catalyst deactivation. However, the ratio between the areas under the bimetallic peak at 40 ° and the PdO (101) peak at 34 ° of the aged sample was calculated to be 0.048 compared to that of 0.062 in the fresh

catalyst, which suggests less bimetallic species relative to oxide present in the aged sample. As highlighted in Figure 5, this decrease in the content of bimetallic species content might also contribute to the observed catalyst deactivation.

The activity of the Pd,Pt,TiO₂/ZSM-5 (80) catalyst was determined in the presence of 9 mL min⁻¹ water in the reaction stream. The activity was observed to decrease slightly in the presence of water with the T_{50%} increasing from 290 °C to 328 °C under dry conditions and in the presence of water respectively, Figure S12 in ESI 8. However, the stability of the catalyst was not significantly affected by the presence of water in the feed. Figure S13 shows the stability of Pd,Pt,TiO₂/ZSM-5 (80) under dry conditions at 300 °C and in the presence of water at 350 °C and the decrease in conversion as shown by the gradient of the graphs does not change with the addition of water. To determine whether the deactivation observed in the presence of water was permanent, after Pd,Pt,TiO₂/ZSM-5 (80) had been run for 43 hours with 9 mL min⁻¹ water in the feed, the feed was transferred to pass directly over the catalyst rather than through the water saturator and the initial activity in the absence of water was again observed, Figure S14. Under these conditions the catalyst showed good stability with the conversion decreasing from 94.4% to 90.4% over 20 hours.

3.4. Is Pd-Pt bimetallic the important protagonist for methane combustion?

To confirm whether or not the Pd-Pt bimetallic species are responsible for the increase in catalytic activity obtained with less acidic supports, a sample in which bimetallic species formation was promoted using a hydrogen pre-treatment step was prepared as described in section 2.2.

The catalytic activity for such a sample was compared with the fresh Pd,Pt,TiO₂/H-ZSM-5 (80) catalyst. Included in the comparison are two other catalysts, one in which 2% Pt was replaced by 2% of Pd leading to a total Pd loading of 7 wt.% and the other where Pd was deposited first followed by calcination, and then by the deposition of Pt and finally by another calcination. The activity profiles of the 4 samples are illustrated in Figure 15 and the summary of XRD is given in Table 5.

The fact that the catalyst in which Pd, Pt were deposited in two consequent steps and the sample with 7% Pd are significantly less active compared to the standard and the H₂-pretreated

Table 5. Summary of XRD data

Catalyst	Average crystallite size (nm)*			Bimetallic /PdO peak area ratio**
	PdO	TiO ₂	Bimetallic	
H ₂ -treated Pd,Pt,TiO ₂ /HZSM-5 (80)	11.9	11.3	31.3	0.32
Aged Pd,Pt,TiO ₂ /H-ZSM-5 (80)	10.4	15.7	40.3	0.048
Standard Pd,Pt,TiO ₂ /H-ZSM-5 (80)	7.6	12.5	38.1	0.062
7%Pd,TiO ₂ /H-ZSM-5 (80)	8.5	13.2	np***	-
Pd,Pt,TiO ₂ /H-ZSM-5 (80) 2-step	8.3	13.1	np***	-

** ratio of the peak area between the bimetallic peak at 40 ° and PdO (101) at ~34 °.*** no bimetallic peak observed.

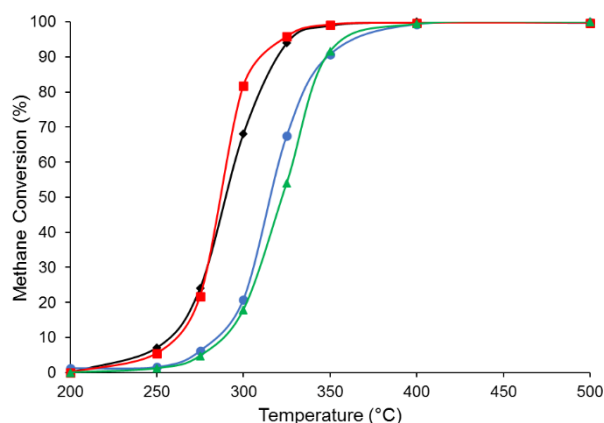


Figure 15. Catalytic activity profiles for methane oxidation over different catalysts. 7 wt.% Pd,TiO₂/H-ZSM-5 (80) (▲), Pd,Pt,TiO₂/H-ZSM-5 (80) prepared in two steps (●), standard Pd,Pt,TiO₂/H-ZSM-5 (80) (◆), and Pd,Pt,TiO₂/H-ZSM-5 (80) with hydrogen pre-treatment (■).

catalysts suggests the simultaneous deposition of Pt and Pd during catalyst synthesis is required in an active catalyst. In addition, the absence of the bimetallic peak in the XRD (last two entries, Table 5) supports this peak being representative of a bimetallic species which is necessary for high activity. Comparing the standard and H₂-treated Pd,Pt,TiO₂/H-ZSM-5 (80) catalysts suggests that the size of PdO does not play an important role in the catalytic activity. Thus, the observed gradual loss of activity over time shown in Figure 14 likely results from the decrease in bimetallic/oxide ratio, specifically from 0.062 in fresh catalyst to 0.048 in the aged sample.

In summary, Figure 16 shows the ratio of the bimetallic to PdO peak areas plotted against the conversion of methane at 300 °C, for all the catalysts shown in Figure 5 and in Table 5. It can be seen that the aged, 2-step and 7 wt.% Pd catalysts fit well into the linear correlation previously found between the bimetallic/PdO ratio and the catalytic activity. The fact that a significant increase in this ratio, achieved with the H₂-treated sample, only resulted in a small improvement in activity suggests the influence of the ratio to the activity has reached its limit.

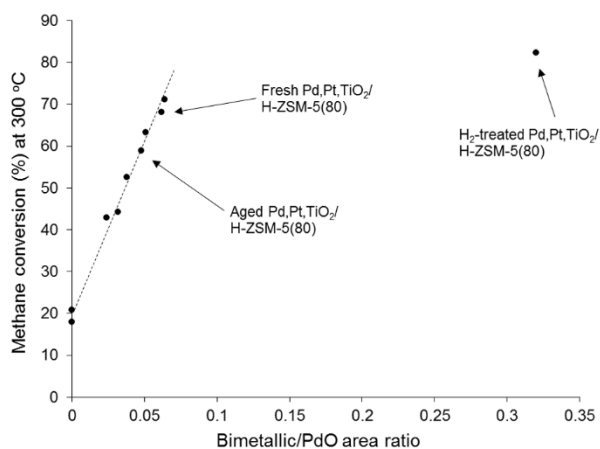


Figure 16. Correlation between the catalytic activity and the bimetallic/PdO ratio.

3. Conclusions

In conclusion, a series of palladium and platinum bimetallic catalysts on TiO₂ and various zeolite supports (H-ZSM-5 of different SiO₂:Al₂O₃ ratios, H-MOR and H-BEA) were synthesized using wet impregnation and tested for the combustion of methane. It is shown that, with similar SiO₂:Al₂O₃ ratios, catalysts prepared on the H-ZSM-5 supports have lower activity compared to that of the H-MOR and H-BEA based catalysts. The catalytic activity of the Pd,Pt,TiO₂/H-ZSM-5 catalysts is found to systematically increase with increase in the SiO₂:Al₂O₃ ratio of the support. NH₃-TPD reveals that, as expected, the amount of acid sites decreases with the increase in SiO₂:Al₂O₃ ratio and suggests that the acid sites of the zeolite do not play an important role in methane activation. Characterization by 2D STEM-EDS and 3D STEM-HAADF tomography shows the high dispersion of palladium and platinum and the fact that palladium and platinum were often co-located on the support. In addition, STEM-HAADF tomography revealed that in Pd,Pt,TiO₂/H-ZSM-5 catalysts, most Pd/Pt particles are located on the external surface of the TiO₂ with TiO₂ sitting on the external, rather than internal, surface of the zeolite, regardless of SiO₂:Al₂O₃ ratio. BET, XRD, ICP-AES, TEM and XAS characterisations confirm that there is minimal difference in the content of palladium, platinum and physical characteristics between the samples supported on H-ZSM-5 of different SiO₂:Al₂O₃ ratios. XAS analysis suggests that palladium and platinum are present mostly as the corresponding oxide nanoparticles/aggregates, which is supported by XPS and XRD analysis. However, analysis of the XRD reveals the formation of a bimetallic phase only in samples in which palladium and platinum were deposited simultaneously. The proportion of the bimetallic phase in Pd,Pt,TiO₂/H-ZSM-5 catalysts is found to increase with decreasing acidity and shows linear correlation with activity. Although the precise nature of the bimetallic phase is unclear, its presence is indicative of species with metallic character and lower oxidation states. This is consistent with the XPS data which shows a shift of the PdO and PtO peaks to lower binding energy and increased metallic character with increasing SiO₂:Al₂O₃ ratio and activity. This more facile redox behaviour is also observed in TPR analysis where a less intense PdO reduction peak is observed for the more active catalysts with higher SiO₂:Al₂O₃ ratios.

Catalysts prepared on H-ZSM-5 of lower SiO₂:Al₂O₃ ratios possess higher stability and the catalyst deactivation is mostly caused by the loss of the bimetallic species. Comparing the H₂-treated catalyst to the fresh catalyst as well as the sequentially impregnated and the 7 wt.% Pd catalysts confirms the importance of the bimetallic species to the activity for total methane oxidation.

Thus, the formation of bimetallic species formed by the close proximity of Pd/Pt was shown to be key in the design of highly active catalysts.

Conflicts of interest

There are no conflicts to declare.

Acknowledgements

T.S.N acknowledges funding from EPSRC through The UK Catalysis Hub (EP/K014706/2) and beamtime from the UK Catalysis Hub BAG (run number sp15151). P.McK acknowledges funding from The Bryden Centre, The Bryden Centre project is supported by the European Union's INTERREG VA Programme, managed by the Special EU Programmes Body (SEUPB). S.J.H. and Y.-C.W. acknowledge funding from the European Research Council H2020 Starter Grant EvoluTEM, EPSRC (EP/P009050/1 and the NowNano CDT), studentship funding from the China Scholarship Council and TEM instruments from the Electron Microscopy Centre at the University of Manchester.

Disclaimer: The views and opinions expressed in this paper do not necessarily reflect those of the European Commission or the Special EU Programmes Body (SEUPB).

References

- H. Rodhe, *Science*, 1990, **248**, 1217.
- Z.-l. Zhou, S.-f. Ji, F.-x. Yin, Z.-x. Lu and C.-y. Li, *Journal of Fuel Chemistry and Technology*, 2007, **35**, 583.
- P. Gélin and M. Primet, *Appl. Catal., B*, 2002, **39**, 1.
- J. Chen, H. Arandiyán, X. Gao and J. Li, *Catalysis Surveys from Asia*, 2015, **19**, 140.
- C. Shi, L. Yang and J. Cai, *Fuel*, 2007, **86**, 106.
- A. Kalantar Neyestanaki and L.E. Lindfors, *Fuel*, 1998, **77**, 1727.
- G. Ercolino, P. Stelmachowski, G. Grzybek, A. Kotarba and S. Specchia, *Appl. Catal., B*, 2017, **206**, 712.
- M. Cargnello, J.D. Jaén, J.H. Garrido, K. Bakmutsky, T. Montini, J.C. Gámez, R. Gorte and P.J.S. Fornasiero, *Science*, 2012, **337**, 713.
- Z. Wu, J. Deng, Y. Liu, S. Xie, Y. Jiang, X. Zhao, J. Yang, H. Arandiyán, G. Guo and H. Dai, *J. Catal.*, 2015, **332**, 13.
- Y. Lou, J. Ma, W. Hu, Q. Dai, L. Wang, W. Zhan, Y. Guo, X.-M. Cao, Y. Guo, P. Hu and G. Lu, *ACS Catal.*, 2016, **6**, 8127.
- J.N. Carstens, S.C. Su and A.T. Bell, *J. Catal.*, 1998, **176**, 136.
- R. Bunting, X. Cheng, J.M. Thompson and P. Hu, *ACS Catal.*, 2019, **9**, 10317.
- O. M'Ramadji, D. Li, X. Wang, B. Zhang and G. Lu, *Catal. Commun.*, 2007, **8**, 880.
- H. Maeda, Y. Kinoshita, K.R. Reddy, K. Muto, S. Komai, N. Katada and M. Niwa, *Appl. Catal., A*, 1997, **163**, 59.
- J.-H. Park, B. Kim, C.-H. Shin, G. Seo, S.H. Kim and S.B. Hong, *Top. Catal.*, 2009, **52**, 27.
- K. Okumura, S. Matsumoto, N. Nishiaki and M. Niwa, *Appl. Catal., B*, 2003, **40**, 151.
- M.J. Truitt, S.S. Toporek, R. Rovira-Hernandez, K. Hatcher and J.L. White, *J. Am. Chem. Soc.*, 2004, **126**, 11144.
- Q. Dai, Q. Zhu, Y. Lou and X. Wang, *J. Catal.*, 2018, **357**, 29.
- A.I. Osman, J.K. Abu-Dahrieh, F. Laffir, T. Curtin, J.M. Thompson and D.W. Rooney, *Appl. Catal., B*, 2016, **187**, 408.
- J. Rouquerol, P. Llewellyn and F. Rouquerol, Is the BET equation applicable to microporous adsorbents?, in: P.L. Llewellyn, F. Rodriguez-Reinoso, J. Rouquerol, N. Seaton (Eds.) *Studies in Surface Science and Catalysis*, Elsevier 2007, pp. 49-56.
- B.D.A. Levin, Y. Jiang, E. Padgett, S. Waldon, C. Quammen, C. Harris, U. Ayachit, M. Hanwell, P. Ercius, D.A. Muller and R. Hovden, *Microscopy Today*, 2018, **26**, 12.
- B. Goris, W. Van den Broek, K.J. Batenburg, H. Heidari Mezerji and S. Bals, *Ultramicroscopy*, 2012, **113**, 120.
- M. Agote-Arán, A.B. Kroner, H.U. Islam, W.A. Sławiński, D.S. Wragg, I. Lezcano-González and A.M. Beale, *ChemCatChem*, 2019, **11**, 473.
- <https://www.alfa.com/en/zeolites/>, 2019.
- R.Q. Long and R.T. Yang, *J. Catal.*, 2001, **198**, 20.
- L. Rodríguez-González, E. Rodríguez-Castellón, A. Jiménez-López and U. Simon, *Solid State Ionics*, 2008, **179**, 1968.
- C.A. González, M. Bartoszek, A. Martin and C.M. de Correa, *Ind. Eng. Chem. Res.*, 2009, **48**, 2826.
- M. Watanabe, Y. Aizawa, T. Iida, R. Nishimura and H. Inomata, *Appl. Catal. A*, 2005, **295**, 150.
- N. Ichikawa, S. Sato, R. Takahashi and T. Sodesawa, *Catal. Commun.*, 2005, **6**, 19.
- K. Persson, A. Ersson, K. Jansson, N. Iverlud and S. Järås, *J. Catal.*, 2005, **231**, 139.
- C.-C. Wang and J.Y. Ying, *Chem. Mater.*, 1999, **11**, 3113.
- S. Ali Ansari, M. Mansoob Khan, M. Omaish Ansari and M. Hwan Cho, *Ceram. Int.*, 2015, **41**, 9131.
- K. Persson, A. Ersson, S. Colussi, A. Trovarelli and S.G. Järås, *Appl. Catal., B*, 2006, **66**, 175.
- Y.-N. Wu, S.-J. Liao, Z.-X. Liang, L.-J. Yang and R.-F. Wang, *J. Power Sources*, 2009, **194**, 805.
- J.S.J. Hargreaves, *Catalysis, Structure & Reactivity*, 2016, **2**, 33.
- M. Kosmulski, *Adv. Colloid Interface Sci.*, 2018, **251**, 115.
- A. Ikhlaiq and B. Kasprzyk-Hordern, *Appl. Catal. B*, 2017, **200**, 274.
- L.S. Kibis, A.I. Stadnichenko, S.V. Koscheev, V.I. Zaikovskii and A.I. Boronin, *J. Phys. Chem. C*, 2012, **116**, 19342.
- T. Pillo, R. Zimmermann, P. Steiner and S. Hüfner, *Journal of Physics: Condensed Matter*, 1997, **9**, 3987.
- T. Wang, R. Yang, S. Ouyang, H. Shi and S. Wang, *RSC Adv.*, 2015, **5**, 48992.
- P. Wu, Y. Huang, L. Kang, M. Wu and Y. Wang, *Sci. Rep.*, 2015, **5**, 14173.
- J.H. Kim, J.Y. Cheon, T.J. Shin, J.Y. Park and S.H. Joo, *Carbon*, 2016, **101**, 449.
- R. Harmsen, S. Bates and R. A. van Santen, *Faraday Discuss.*, 1997, **106**, 443.
- L.L. Sheu, H. Knoezinger and W.M.H. Sachtler, *J. Am. Chem. Soc.*, 1989, **111**, 8125.
- A.K. Khudorozhkov, I.A. Chetyrin, A.V. Bukhtiyarov, I.P. Prosvirin and V.I. Bukhtiyarov, *Top. Catal.*, 2017, **60**, 190.
- B. Wen, J. Jia and W.M.H. Sachtler, *J. Phys. Chem. B*, 2002, **106**, 7520.
- C.-B. Wang, C.-M. Ho, H.-K. Lin and H.-C. Chiu, *Fuel*, 2002, **81**, 1883.
- C.-P. Hwang and C.-T. Yeh, *J. Mol. Catal. A: Chem.*, 1996, **112**, 295.
- W. Lin, Y.X. Zhu, N.Z. Wu, Y.C. Xie, I. Murwani and E. Kemnitz, *Appl. Catal., B*, 2004, **50**, 59.